Properties of YNi_2B_2C superconducting thin films

R. Vaglio, A. Andreone, C. Aruta, A. Cassinese, and F. Fontana*
Istituto Nazionale per la Fisica della Materia (INFM), Dipartimento di Scienze Fisiche, Università di Napoli Federico II, Piazzale Tecchio 80, I-80125 Napoli, Italy

G. W. Crabtree, M. Iavarone,† and Y. De Wilde
Materials Science Division-Science and Technology Center for Superconductivity, Argonne National Laboratory, Argonne, Illinois 60439

L. Maritato, C. Attanasio, C. Coccorese, M. Salluzzo, and M. Salvato
Dipartimento di Fisica, Università di Salerno, I-84081 Baronissi (Salerno), Italy
(Received 20 January 1997)

High-quality, *c*-axis-oriented thin films of the intermetallic superconductor YNi_2B_2C were obtained *in situ* by magnetron sputtering on MgO and other substrates held at about $T=800\,^{\circ}C$. The best films showed a maximum of $T_c=15.1$ K with $\Delta T_c \approx 0.1$ K. We report on structural and electrical film characterization including dc resistivity measurements up to 450 K as well as critical-field and critical-current measurements. Scanning tunnel microscope tunneling measurements were also performed, giving further evidence of the overall BCS nature of these compounds. [S0163-1829(97)07325-6]

I. INTRODUCTION

Intermetallic compounds of the class R-Ni_2B_2C (R=rare earth) (Refs. 1 and 2) have recently attracted the attention of researchers due to their intriguing superconducting and magnetic properties. They present an anisotropic layered structure, as high-T_c oxide superconductors, and a strong interplay between superconductivity and magnetism.[3,4] Though many papers appeared in the literature concerning the properties of these compounds in polycrystalline bulk or single-crystal form, only very few papers appeared on thin-film preparation and properties.[5,6]

In the present paper we present a wide characterization of *in situ* grown films of the superconducting compound YNi_2B_2C. Measurement of dc transport properties, critical fields and currents as well as scanning tunnel microscope (STM) tunneling were performed. Most of the reported measurements derive significant advantage from the highly textured, thin-film form of the samples.

II. FILM PREPARATION AND STRUCTURAL CHARACTERIZATION

YNi_2B_2C films were prepared by a planar magnetron sputtering technique as described in Ref. 6.

A 2-in-diam, 6-mm-thick YNi_2B_2C target was prepared by arc melting stoichiometric amounts of raw materials on a water-cooled cylindrical copper niche under a dry argon atmosphere. Four melting passes ensured good homogeneity, the overall weight loss being less than 0.5%. Following melting, the target was gently machined to produce a reasonably flat, crack-free disk.

Electron microscopy inspection revealed the absence of significant unalloyed elements (1% level). X-ray photoemission spectroscopy (XPS) analyses confirmed the target stoichiometric composition and x-ray-diffraction (XRD) data showed the superconducting YNi_2B_2C phase with no detectable impurity phase.

The substrates were placed ''on axis'' at 9 cm from the target surface and could be heated up to about 1000 °C by means of a molybdenum heater. MgO, (100) oriented, as well as sapphire (Al_2O_3), and $LaAlO_3$ substrates were used in this study. The base system pressure P_{in} just before sputtering was in the low 10^{-5} Pa range. The film thickness was monitored during growth by a quartz oscillator. The final thickness was set close to 500 nm for all depositions.

A key role in obtaining high-quality films was played by the substrate temperature T_s (measured by a thermocouple glued at the surface of a side substrate)[6] as well as by the Ar partial pressure P_{Ar}, which had to be sufficiently high to avoid resputtering effects. Though superconducting films were obtained on all substrates, high-quality films ($T_c \geqslant 15$ K, resistivity ratio $[RRR=\rho(300\,K)/\rho_0] \geqslant 5$) were reproducibly obtained only on MgO substrates.

The optimized process parameters are reported in Table I.

As reported in Fig. 1, the x-ray ϑ-2ϑ diffraction pattern for the optimized films revealed the predominant presence of $(00n)$ YNi_2B_2C reflections. This indicates a strong preferential orientation along the *c* axis. The rocking curve around the (004) reflection gave a full width at half maximum (FWHM)=1.2°. From the $(00n)$ reflections, we can estimate $c=1.063$ nm, and from the weak (112) reflection, we get $a=0.353$ nm, both close to the bulk values.

In Fig. 1 we also see some Y_2O_3 peaks, tentatively attrib-

TABLE I. Main parameters for YNi_2B_2C films grown with dc magnetron sputtering technique. V and I are the voltage and the discharge current of the sputtering process respectively.

P_{in} (Pa)	P_{Ar} (Pa)	T_s (°C)	V (V)	I (A)	Rate (nm/s)
10^{-5}	3	≈800	400	0.8	0.8

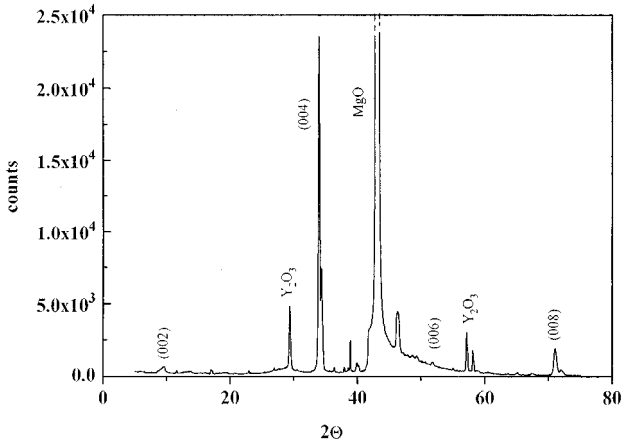

FIG. 1. X-ray ϑ-2ϑ diffraction pattern for a YNi_2B_2C film on a MgO substrate.

uted to partial oxidation of the sample surface, as well as other minor impurity phases.

In Fig. 2 scanning electron microscopy (SEM) pictures of the samples surface are reported on different scales. The films appear to be granular with typical grain sizes between

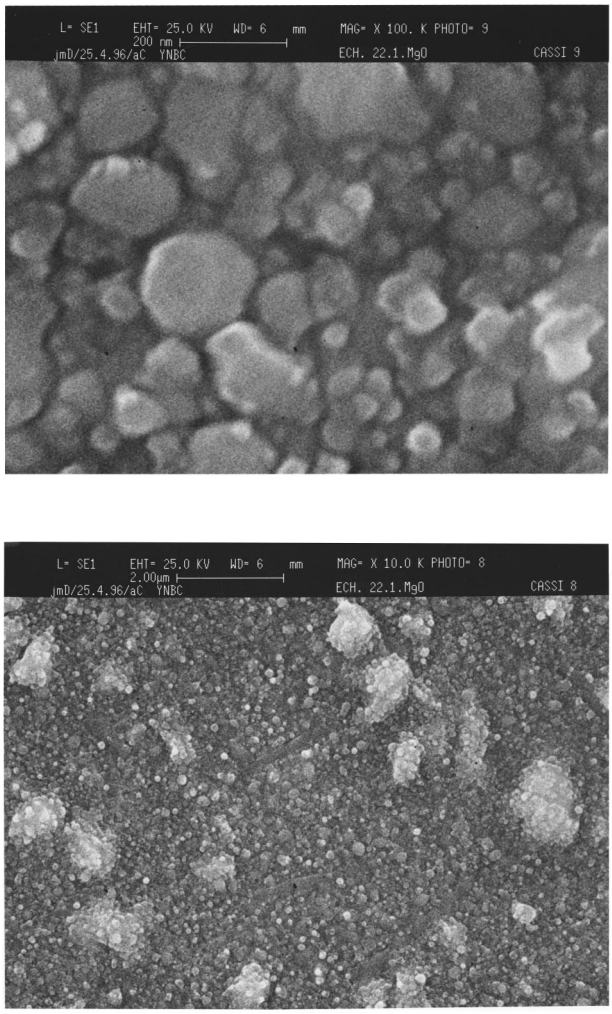

FIG. 2. SEM pictures of a YNi_2B_2C film deposited on a MgO substrate (a) The scan area is 1.15 μm $\times$ 0.78 μm; (b) the scan area is 11.5 μm $\times$ 7.8 μm.

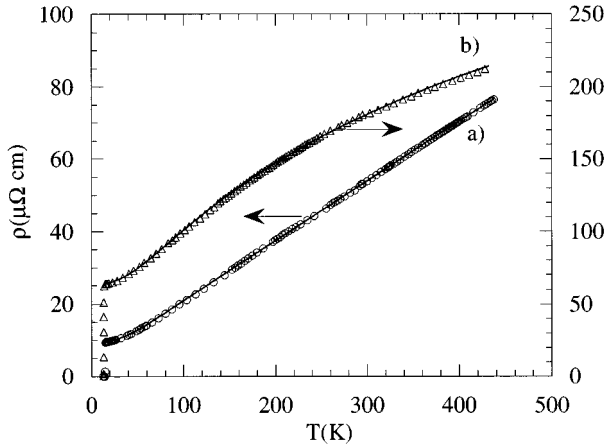

FIG. 3. (a) Resistivity vs temperature for one of the best YNi_2B_2C films, grown on a MgO substrate, up to $T=450$ K (open circles), together with the fitting curve (solid line) which gives $n=2$, $\vartheta_d=330\pm20$ K, $\rho'=0.17\pm0.01$; (b) resistivity vs temperature for a lower-quality YNi_2B_2C film, grown on a $LaAlO_3$ substrate, up to $T=450$ K (open triangles) together with the fitting curve (solid line) which gives $n=2$, $\vartheta_d=330\pm20$ K, $\rho'=0.50\pm0.01$, and $\rho_s=460\pm30$ $\mu\Omega$ cm.

50 and 200 nm. The large bright aggregates that can be identified in Fig. 2(a) correspond to the presence of insulating Y_2O_3, confirming the X-ray-diffraction indications.

From XPS measurements it can be seen that Y_2O_3 oxide is only present in the first 20–30 nm from the surface and that the correct 1:2:2:1 composition is recovered in the bulk of the sample.

III. dc RESISTIVITY MEASUREMENTS

In Fig. 3 the film dc resistivity as a function of the temperature up to $T=450$ K is reported for high-quality and lower-quality films, respectively. The absolute value of the resistivity was determined using a commercial linear four-probe head (tip spacing=0.65 mm). The absolute error, mainly associated with the thickness measurement, performed by a standard profilometer, is estimated to be of the order of 5%. The critical temperature defined by the 10%–90% criterion is $T_c=15.1$ K, close to the bulk value.[1,2]

As in most transition metals and alloys, the temperature dependence of the normal-state resistivity of our YNi_2B_2C films is well described by the expression

$$\rho(T)=\{[\rho_0+\rho_{\rm ph}(T)]^{-1}+\rho_s^{-1}\}^{-1} \tag{1a}$$

where ρ_0 is related to impurities or defects,

$$\rho_{\rm ph}(T)=(n-1)\rho'\,\theta_D\left(\frac{T}{\theta_D}\right)^n\int_0^{\theta_D/T}\frac{x^n dx}{(e^x-1)(1-e^{-x})} \tag{1b}$$

represents a generalized Block-Grüneisen expression for the electron-phonon contribution, and ρ_s represents a ''saturation value'' related to the existence of a minimum value for the mean free path.[7] Since $\rho_0 \ll \rho_s$, $\rho(0\,{\rm K})\approx\rho_0$ so that ρ_0 can be identified with the residual resistivity.

The resistivity vs temperature of the best films up to $T=450$ K can be well fitted by Eqs. (1) assuming $n=2$, ϑ_d

$=330\pm20$ K, $\rho'=(0.17\pm0.01)$ $\mu\Omega$ cm/K and 10 $\mu\Omega$ cm $\leqslant\rho_0\leqslant30$ $\mu\Omega$ cm depending on the film quality. The measured ρ_0 values compare well with single-crystal data[8] and are much lower than what is reported for *ex situ* films[5] or polycrystalline samples. These films do not show any saturation up to 450 K.

These data require a detailed comment. First of all, it appears that the normal-state resistivity is clearly determined by electron-phonon scattering. The T^2 dependence of the resistivity is consistent with data on YNi_2B_2C single crystals.[8] This behavior has been attributed to electron-electron correlation effects,[8] but in our opinion is more likely to be attributed to the fairly strong electron-phonon interaction, which, together with the presence of some structural disorder, has been proved to determine an $n=2$ exponent in the low-temperature dependence of resistivity in many type-II superconductors.[9] However, according to Ref. 9, given our ρ_0 values, this would imply a rather high value of the electron-phonon interaction constant $\lambda(\lambda\geqslant1.1)$.

The value obtained for the Debye temperature is lower than some estimations from specific heat data,[10] but is not far from other determination.[11] Inserting our ϑ_d and T_c values in the McMillan formula[12] and assuming as usual $\mu^*=0.10$–0.15, we yield for the electron-phonon interaction parameter the value $\lambda=1.0\pm0.1$.

This value, together with the measured ρ', can give an estimation of the plasma frequency Ω_p through the relation[9]

$$\lambda_{\rm tr}=0.246(\hbar\Omega_p)^2\rho', \tag{2}$$

where ρ is expressed in $\mu\Omega$ cm and $\hbar\Omega_p$ in eV. Assuming $\lambda=\lambda_{\rm tr}$,[12] this leads to $\hbar\Omega_p\approx4.9$ eV which is very close to other estimations.[13,14]

The resistivity vs temperature curves for lower quality films can be still fitted by Eqs. (1). In this case, due to the high value of the resistivity, saturation effects are observed. A typical resistivity vs temperature curve is reported in Fig. 3 [curve (b)] together with the fitting curve. From the obtained value $\rho_s=460\pm30$ $\mu\Omega$ cm we can evaluate the minimum mean free path $l_{\rm min}$ through the relation[7]

$$\rho_{\rm sat}=\frac{4\pi v_F}{(\hbar\Omega_p)^2 l_{\rm min}}. \tag{3}$$

By taking into account the Fermi velocity value ($v_F=2.12\times10^7$ cm/s) worked out from band structure calculations,[13] we obtain $l_{\rm min}\approx0.3$ nm, which compares well with typical interatomic distances.

Finally it is very instructive to plot the measured T_c values for our YNi_2B_2C films (including nonoptimized samples) as a function of RRR. This is reported in Fig. 4. Though the statistics is limited, for all films the T_c-RRR relation seems to follow the same ''universal'' relation observed for Nb and $A15$ compounds,[15] indicating that the high T_c in borocarbides is related to the presence of a peak at the Fermi energy in the density of states. This confirms the results of band structure calculations[16,17] and experimental evidence based on the results of substitutions on the Ni site,[18] and gives further evidence that electron correlation effects, hypothesized from photoemission studies,[19,20] are not relevant in these compounds.

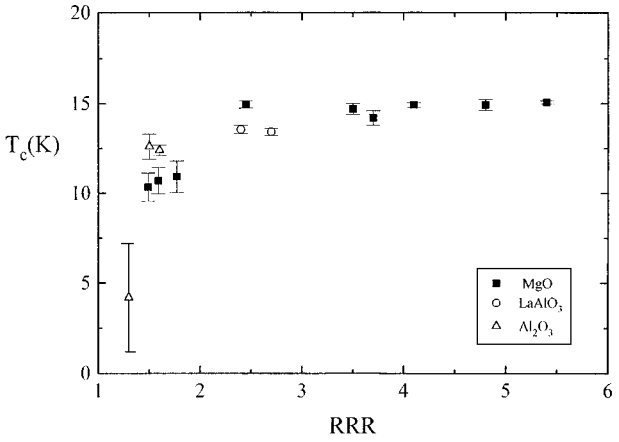

FIG. 4. Critical temperature T_c as a function of the residual resistivity ratio RRR for YNi_2B_2C films grown on different substrates.

IV. CRITICAL-CURRENT AND CRITICAL-FIELD MEASUREMENTS

For the critical-current and critical-magnetic-field measurements, the films were mounted on a copper block and kept in close thermal contact with a thermometer suitable for high-magnetic-field measurements. The critical-current values were obtained using a dc four-probe method with a voltage criterion of 5 μV. A superconducting solenoid with a high-field uniformity was used for the measurements performed in both the parallel and perpendicular directions with respect to the plane of the films. The experimental setup allowed measurements in the temperature range 4.2–300 K with an externally applied magnetic field up to 5 T.

In Fig. 5 are shown the temperature behaviors of the parallel $H_{c2\parallel}$ and the perpendicular $H_{c2\perp}$ magnetic fields for a sample with $T_c=15.1$ K in zero field. In the investigated temperature range, both curves show a slight upward curvature already seen in previous reports.[21] In the inset the tran-

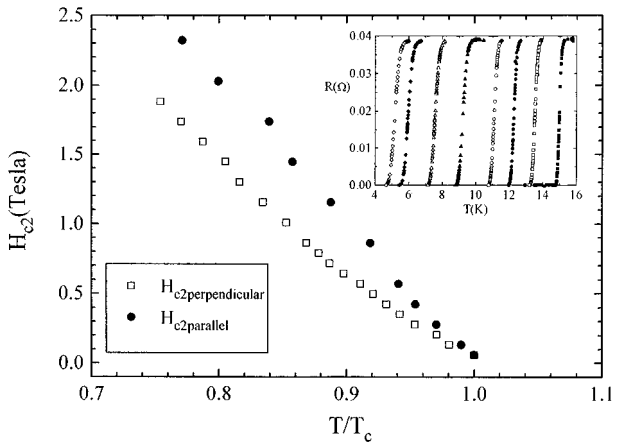

FIG. 5. Critical magnetic field H_{c2} versus the reduced temperatures $t=T/T_c$ for the same sample in Fig. 1 in the case of parallel (circles) and perpendicular (squares) external fields. In the inset the transition curves for different values of the perpendicular external magnetic fields ($H=0.06$, 0.28, 0.50, 0.72, 1, 1.3, 1.60, and 1.74 T) are shown. The critical temperature, in zero field, for this sample is $T_c=15.1$ K.

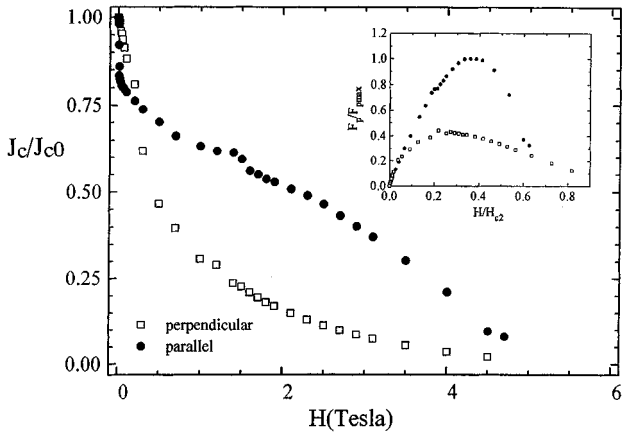

FIG. 6. Normalized critical-current density curves in perpendicular (squares) and parallel (circles) external fields. The critical-current density value in zero field at 4.2 K is $J_{c0}=9.5\times10^4$ A/cm^2. The inset shows the normalized pinning forces vs the reduced field $h=H/H_{c2}$ in the parallel (circles) and perpendicular (squares) field directions.

sition curves at different perpendicular magnetic fields are shown. Even at high magnetic fields, we did not observe the presence of a tail in the low-temperature part of these curves, suggesting strong pinning in these films even close to H_{c2}.

From the critical field slope, we can estimate $\xi_\perp=(6.1\pm0.5)$ nm, $\xi_\parallel=(8.0\pm0.5)$ nm, and an anisotropy ratio $\gamma=\xi_\parallel/\xi_\perp=(m_\perp/m_\parallel)^{1/2}\approx1.3$. This agrees fairly well with previous determinations,[8,21] though other reports on single crystals give $\gamma\approx1$.[22,23]

In Fig. 6 is shown the magnetic-field dependence of the critical-current density with perpendicular and parallel external magnetic fields. In the inset the normalized pinning forces for parallel and perpendicular applied magnetic fields are shown. It is interesting to point out that in the low-magnetic-field region, the J_c values in the perpendicular fields are higher than those in the parallel fields. At a magnetic field of about 0.3 T, the two curves cross each other. Assuming the presence of columnar grains, the strongest pinning centers in both the perpendicular and parallel directions are related to nonsuperconducting zones. At low magnetic fields, the perpendicular pinning energies, proportional to the thickness of the films, are higher than the parallel pinning energies, proportional to the average grain dimension D in the plane of the films. When the average distance between vortex lines in a perpendicular field $a_0=(\phi_0/B)^{1/2}$ starts to be lower than D, vortices penetrate into the grains, resulting in weaker perpendicular pinning forces. As a consequence, J_c values in parallel fields start to be higher than those in perpendicular fields. From the field value at the crossing point, it is then possible to extrapolate a typical value for D. In our case we get $D\approx(\phi_0/0.3T)^{1/2}=80$ nm which is in good agreement with values obtained by SEM.

The J_c behavior in parallel fields higher than 0.3 T is similar to what is observed for layered systems as NbN/AlN (Ref. 24), Mo/V, and Nb/Pd (Ref. 25) multilayers.

V. STM TUNNELING MEASUREMENTS

Besides the aforementioned SEM and XPS measurements, a low-temperature scanning tunneling microscope (STM) has been used to characterize the YNi_2B_2C thin films on a smaller scale. This technique allows us not only to obtain topographic information, but also provides a powerful spectroscopic tool, giving a direct local probe of the quasiparticle density of states (DOS).

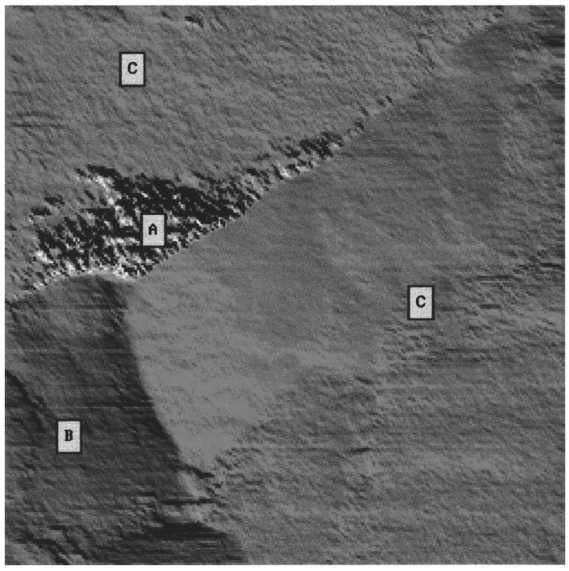

FIG. 7. Topographic image of YNi_2B_2C thin film at 4.2 K obtained in the constant-current mode. The scan area is 500 Å$\times$500 Å, and the imaging parameters are $I=70$ pA and $V=30$ mV.

Other tunneling measurements have already been performed on polycrystalline YNi_2B_2C samples using STM (Refs. 26 and 27) and break junctions.[28] Point-contact spectroscopy has been also used to infer the gap value.[29,30]

The measurements reported below were performed at the Argonne National Laboratory with a home-built, low-temperature STM operating in a helium exchange gas at 4.2 K. The STM is combined with RHK electronic software (RHK Technology-STM 100). Using a lock-in amplifier, the system allows measurements of conductance vs voltage (dI/dV vs V) characteristics at selected points simultaneously with the recording of the surface topography. No surface treatment was applied to the samples prior to mounting on the STM. The tip was made of Pt-Ir wires sharpened mechanically with scissors.

Figure 7 shows a typical topographic image on a scale of 500 Å by 500 Å acquired in the constant-current mode. Several subsequent scans were performed over this area and showed an absolute reproducibility of the topographic features, which is a signature of vacuum tunneling. The topography is granular, analogous to that seen in SEM measurements on a larger scale (Fig. 2). Spectroscopic dI/dV vs V curves have been measured between -20 and 20 mV all over this area. Three different regions, denoted A, B, and C in Fig. 7, are observed. Each region exhibits a distinct spectroscopic behavior which changes abruptly when passing from one region to another. Region A has an insulating behavior characterized by the absence of tunneling current. Region B shows a metallic behavior with a flat or slightly parabolic dI/dV vs V dependence typical for NIN junctions.[31] In what follows we focus our study on region C where we reproducibly observe a well-defined peaked structure related to the superconducting energy gap.

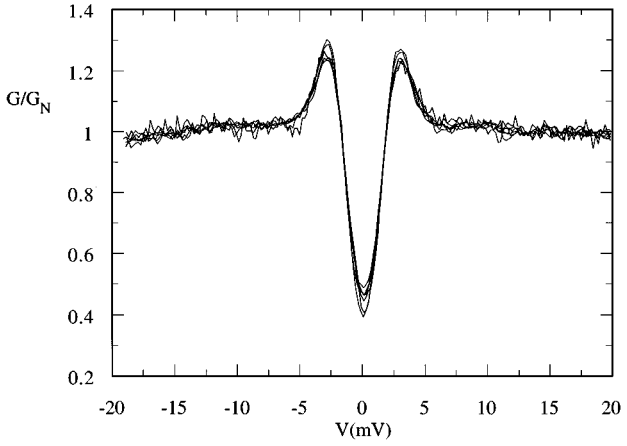

FIG. 8. Normalized conductance vs voltage spectra measured at $T=4.2$ K for different values of the tunneling resistance $R_t=12.5$ MΩ, 25 MΩ, 50 MΩ, 0.1 GΩ, 0.2 GΩ, and 0.4 GΩ.

To ensure vacuum tunneling conditions, all the spectroscopic curves were recorded at a resistance equal to or higher than that of the corresponding topographic image. They are spatially reproducible within the same superconducting region and independent of the value of the tunneling resistance. Figure 8 represents a series of normalized dI/dV vs V curves for tunneling resistances ranging from 10 MΩ to 0.4 GΩ, showing the absolute reproducibility of the data. This constitutes a meaningful check of the junction quality. In Fig. 9 we present the dependence of the tunnel current I as a function of the tip-sample distance d. The exponential decay of the current is another strong indication for vacuum tunneling, for which $I\propto\exp(-1.025\sqrt{\Phi}d)$ is expected, where Φ is the apparent work function.[32] Using this expression for the current to fit our data, we obtain a value of Φ around 1 eV. Such a high value of Φ for this type of STM measurement[33] is explained by a clean tunnel junction without intermediate states in the barrier due to surface contamination, adsorbates, or oxide layers on the tip and/or sample surface.[34]

The characteristic presented in Fig. 10 is the result of the

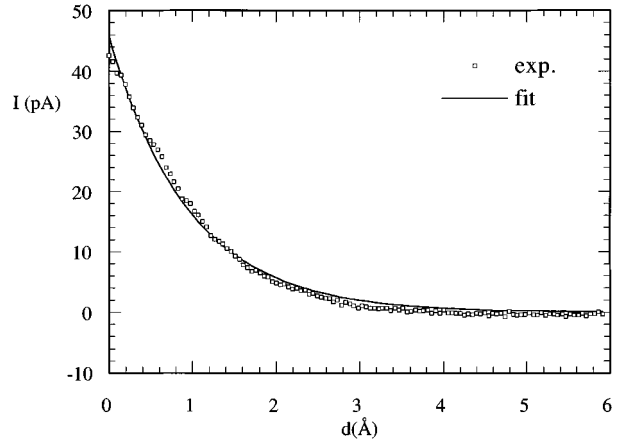

FIG. 9. Variation of the tunneling current I_t as a function of the tip-sample spacing d. The squares represent the experimental data, while the solid curve is the result of an exponential fit giving $\Phi=1$ eV (see text).

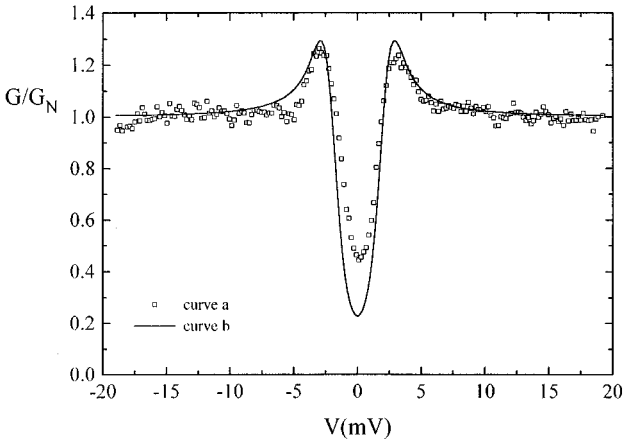

FIG. 10. Normalized experimental conductance [curve (a)] and calculated conductance curves at 4.2 K using a smeared BCS DOS [curve (b)]. The fitting parameters are $\Delta=2.1$ meV and $\Gamma=0.4$ meV.

averaging of 20 individual dI/dV vs V characteristics recorded at the same spot, after normalization by a slightly parabolic background. This normalization procedure was adopted after verification that only this type of background remains when a magnetic field of 6 T is applied in order to suppress the superconductivity in the sample. At low temperature the tunneling conductance in a *NIS* junction can be expressed by

$$\frac{dI(V)}{dV}\propto\int_{-\infty}^{\infty}N(E)\left\{-\frac{\partial}{\partial eV}f(E+eV)\right\}dE\cong N(eV), \quad (4)$$

where $f(E)=1/\{\exp(E/k_BT)+1\}$ is the Fermi function, e the elementary charge, and $N(E)$ the density of states of the superconducting sample.

Fitting the data with this expression and a smeared version of the BCS DOS,

$$N(E)=\mathrm{Re}\{|E-i\Gamma|/[(E-i\Gamma)^2-\Delta^2]^{1/2}\},$$

which includes a broadening parameter Γ,[35] yields curve (b) in Fig. 10. The fit is adjusted for a best matching of the peaks in the experimental curve. The resulting fitting parameters are $\Delta=2.1$ meV and $\Gamma=0.4$ meV. There is still a slight discrepancy with respect to the zero-bias conductance value, which seems to indicate that another mechanism besides the finite lifetime of the quasiparticle might contribute to the tunnel current. Combined with a value of $T_c=15.1$ K, the corresponding BCS ratio $2\Delta/k_BT_c$ is equal to 3.2 ± 0.2.

These values are compatible with what has already been observed in the literature,[28,29] which confirms the substantial weak-coupling nature of YNi_2B_2C.

VI. CONCLUSIONS

In the present paper we have discussed the properties of sputter-deposited, high-quality, c-axis-oriented YNi_2B_2C films.

The resistivity measurements show that YNi_2B_2C is a good metal (RRR higher than 5) with normal-state transport properties dominated by e-ph scattering. The T^2 dependence observed at low temperature is likely to be associated with

the high e-ph interaction constant ($\lambda \approx 1$) and disorder, more than to correlation effects. Moreover, the film resistivity tends to saturate at high temperatures, when the mean free path approaches interatomic distances.

Critical-field measurements showed that, despite the layered crystal structure, YNi_2B_2C is only moderately anisotropic. The critical current in the film is limited by grain boundary effects and related to the granular nature of our samples, consistently to the SEM measurements.

Tunneling measurements performed with a low-temperature STM show a BCS-like density of states with $\Delta = 2.1$ meV and a lifetime broadening parameter $\Gamma = 0.4$ meV (not necessarily intrinsic). This gives a value $2\Delta/K_B T_c \approx 3.2$, which is consistent with the e-ph constant λ estimated by the McMillan T_c formula or by transport measurements ($\lambda \approx 1$).

The overall emerging picture is that YNi_2B_2C is a moderately anisotropic metal, exhibiting s-wave, BCS conventional superconductivity.

ACKNOWLEDGMENTS

The authors wish to thank C. Ferdeghini and S. Siri for discussions and suggestions, P. Manini, and E. Cogliati for the target preparation, G. Gemme (INFN Genova) for XPS analysis, M. Valentino for XRD measurements, and V. Metlushko for his contribution in the characterization of the samples. The technical support of A. Maggio, S. Marrazzo, and S. Avallone is also acknowledged. This work was supported by the U.S. DOE Basic Energy Science-Material Science Department under Contract No. W-31-109-ENG-38 (G.W.C., M.I.) and the NSF Science and Technology Center for Superconductivity under Contract No. DMR 91-2000 (Y.D.W.).

*Also at Università del Molise, SAVA Department, Campobasso, Italy.

†Permanent address: Dipartimento di Scienze Fisiche, Università di Napoli Federico II, Napoli, Italy.

[1] R. J. Cava, H. Takagi, H. W. Zandbergen, J. J. Krajewski, W. F. Peck, Jr., T. Siegrist, B. Batlogg, B. van Dover, R. J. Felder, K. Mizuhaski, J. O. Lee, H. Eisaki, and S. Uchida, Nature (London) **367**, 252 (1994).

[2] R. Nagarajan, C. Mazumdar, Z. Hossian, S. K. Dhar, K. V. Gopalakrishnan, L. C. Gupta, C. Godart, B. D. Padalia, and R. Vijayraghavan, Phys. Rev. Lett. **72**, 274 (1994).

[3] H. Eisaki, H. Takagi, R. J. Cava, B. Batlogg, J. J. Krajewski, W. F. Peck, Jr., K. Mizuhashi, J. O. Lee, and S. Uchida, Phys. Rev. B **50**, 647 (1994).

[4] B. K. Cho, P. C. Canfield, and D. C. Johnston, Phys. Rev. Lett. **77**, 163 (1996).

[5] S. Arisawa, T. Hatano, K. Hirata, T. Mochinu, H. Kitaguchi, H. Fujii, H. Kumakura, K. Kadowaki, K. Nakamura, and K. Togano, Appl. Phys. Lett. **65**, 1299 (1994).

[6] A. Andreone, M. Iavarone, R. Vaglio, P. Manini, and E. Cogliati, Appl. Phys. Lett. **69**, 118 (1996).

[7] M. Gurvitch, Phys. Rev. B **34**, 540 (1986).

[8] H. Takagi, R. J. Cava, H. Eisaki, S. Uchida, J. J. Krajewski, and W. F. Peck, Jr., in *Proceedings of the 7th International Symposium on Superconductivity*, edited by K. Tamafuji and T. Morishita (Springer, Berlin, 1995), p. 9.

[9] M. Gurvitch, Physica B **135**, 276 (1985).

[10] C. Godart, L. C. Gupta, R. Nagarajan, S. K. Dhar, H. Noel, M. Potel, C. Mazumdar, Z. Hossain, C. Levy-Clement, G. Schiffmacher, B. D. Padalia, and R. Vijayaraghavan, Phys. Rev. B **51**, 489 (1995).

[11] S. A. Carter, B. Batlogg, R. J. Cava, J. J. Krajewski, W. F. Peck, Jr., and H. Takagi, Phys. Rev. B **50**, 4216 (1994).

[12] W. L. McMillan, Phys. Rev. **167**, B331 (1967).

[13] W. E. Pickett and D. J. Singh, Phys. Rev. Lett. **72**, 3702 (1994).

[14] K. Widder, D. Berner, A. Zibold, H. P. Geserich, M. Knupper, M. Kielwein, M. Buchgeister, and J. Fink, Europhys. Lett. **30**, 55 (1995).

[15] L. R. Testardi and L. F. Mattheiss, Phys. Rev. Lett. **41**, 1612 (1978).

[16] L. F. Mattheis, Phys. Rev. B **49**, 13 279 (1994).

[17] H. Kim, C. Hwang, and J. Ihm, Phys. Rev. B **52**, 4592 (1995).

[18] A. K. Gangopadhyay, A. J. Schuetz, and J. S. Schilling, Physica C **246**, 317 (1995).

[19] A. Fujimori, K. Kobayashi, T. Mizokawa, K. Mamiya, A. Sekiyama, H. Eisaki, H. Takagi, and W. F. Peck, Jr., Phys. Rev. B **50**, 9660 (1994).

[20] K. Kobayashi, T. Mizokawa, K. Mamiya, A. Sekiyama, A. Fujimori, H. Takagi, S. Uchida, R. J. Cava, J. J. Krajewski, and W. F. Peck, Jr., Phys. Rev. B **54**, 507 (1996).

[21] M. Baron, L. Gladezuk, J. Gorecka, M. Szymczak, R. Szymczak, Z. Drzazga, and M. Winiarska, J. Magn. Magn. Mater. **136**, L1 (1994).

[22] M. Xu, B. K. Cho, P. C. Canfield, D. K. Finnemore, and D. C. Johnston, Physica C **235**, 2533 (1994).

[23] E. Johnston-Halperin, J. Fizder, D. E. Farrel, M. Xu, B. K. Cho, P. C. Canfield, D. K. Finnemore, and D. C. Johnston, Phys. Rev. B **51**, 12 852 (1995).

[24] K. E. Gray, R. T. Kampwirth, D. J. Miller, J. M. Murduck, D. Hampshire, R. Herzog, and H. W. Weber, Physica C **174**, 340 (1991).

[25] D. G. de Groot, A. J. Vemeer, C. W. Hagen, T. A. M. Schroder, N. J. Koeman, J. H. Rector, R. Griessen, M. G. Karkut, J. M. Triscone, and O. Fischer, Vacuum **41**, 1244 (1990).

[26] E. Bar-Sadeh, I. Felner, U. Asaf, and O. Millo, Phys. Rev. B **52**, 6734 (1995).

[27] G. T. Jeong, J. I. Kye, S. H. Chun, Z. G. Khim, W. C. Lee, P. C. Canfield, B. K. Cho, and D. C. Johnston, Physica C **253**, 48 (1995).

[28] T. Ekino, H. Fujii, M. Kosugi, Y. Zenitani, and J. Akimitsu, Phys. Rev. B **53**, 5640 (1996).

[29] A. Andreone, F. Fontana, M. Iavarone, R. Vaglio, F. Canepa, P. Manfrinetti, and A. Palenzona, Physica C **251**, 379 (1995).

[30] L. F. Rybaltchznko, I. K. Janson, A. G. M. Jansen, P. Mandal, P. Wider, C. V. Tomy, and D. McPaul, Physica B **218**, 189 (1996).

[31] J. G. Simmons, J. Appl. Phys. **34**, 2581 (1963).

[32] E. L. Wolf, *Principles of Electron Tunneling Spectroscopy* (Oxford University Press, New York, 1985).

[33] Ch. Renner and Ø. Fisher, Phys. Rev. B **51**, 9208 (1996).

[34] J. Halbritter, G. Repphun, S. Vinzelberg, G. Staikov, and W. J. Lorenz, Electrochim. Acta **40**, 1385 (1995).

[35] R. C. Dynes, V. Narayanamurti, and J. P. Garno, Phys. Rev. Lett. **41**, 1509 (1978).